Soft Matter

PAPER

View Article Online
View Journal | View Issue

Cite this: *Soft Matter*, 2016, 12, 2301

An optimized protocol for the analysis of time-resolved elastic scattering experiments

Michelle A. Calabrese, Norman J. Wagner and Simon A. Rogers*†

Received 15th December 2015,
Accepted 4th January 2016

DOI: 10.1039/c5sm03039k

www.rsc.org/softmatter

A deconvolution protocol is developed for obtaining material responses from time-resolved small-angle scattering data from light (SALS), X-rays (SAXS), or neutrons (SANS). Previously used methods convolve material responses with information from the procedure used to group data into discrete time intervals, known as binning. We demonstrate that enhanced signal resolution can be obtained by using methods of signal processing to analyze time-resolved scattering data. The method is illustrated for a time-resolved rheo-SANS measurement of a complex, structured surfactant solution under oscillatory shear flow. We show how the underlying material response can be clearly decoupled from the binning procedure. This method greatly reduces the experimental acquisition time, by approximately one-third for the aforementioned rheo-SANS experiment.

Introduction

The study of soft matter is a multidisciplinary and active area of research that often includes materials with time-dependent structures, resulting from self-assembly, phase transitions or an external excitation, such as a shear or electromagnetic field. Accessing structural information on the relevant length scales in soft matter science can be achieved through light, X-ray, or neutron scattering. During a scattering experiment, a beam of particles of a specified wavelength is directed onto the material of interest. This elastic scattering is collected at a detector that records the spatial position of the particle and the time of acquisition. Scattering from stationary or steady-state materials provides microstructural information about the quiescent or locally time-independent state; thus the material properties can be represented by the time-average over the experimental period, T. However, there has been a recent increase of interest surrounding time-resolved scattering experiments, where materials such as biological macromolecules,[1,2] gels,[3–5] vesicles and membranes,[6–8] polymers and polymer crystal phases,[9,10] and micelle solutions[11–14] have been investigated. The structure of materials responding to an applied excitation should not be analyzed by this simple time-average of the scattering, as the time-dependent nature of the response cannot be discerned. Accordingly, the development of new methods to analyze time-dependent scattering data is essential to both accurately and efficiently determine the true temporal material response.

Time-dependent scattering is often analyzed by an averaging procedure known as 'binning.' The binning procedure groups the scattering information into fixed intervals (bins) of duration t_w, referred to as the bin width. Here, the material response is examined on a timescale much shorter than that of the full experiment, $t_w \ll T$. By dividing the scattered particles into discrete time bins, the material properties are averaged over t_w and are assumed to be relatively constant within the bin. For example, in a scattering experiment of 30 minute duration (T = 30 min), researchers may choose to examine the structural changes after every minute (t_w = 1 min). In this case, the average material structure per one-minute time bin is analyzed.

In order for such analysis to be performed, the detector must time-stamp each detected particle in addition to recording its spatial position. Fig. 1 shows an example data set, where the X and Y position on the detector and the time of detection for each scattering event are shown in three dimensions for a typical small angle neutron scattering (SANS) experiment. The red data points in Fig. 1 represent neutrons scattered during a cycle of an oscillatory shear experiment of period T, so that the time axis is normalized as t/T. The spatial and temporal dependence of the scattering events leading to this detector response, as shown in Fig. 1, is indicative of the continuously varying dynamics inherent to the system of interest.

In the standard binning method, three dimensional spatially- and temporally-resolved data are reduced to a sequence of two-dimensional patterns, where the detector response to the scattering is grouped into non-overlapping time bins of duration t_w. As shown in Fig. 1, the detected scattering events are binned with $t_w = T/10$ (between black or colored lines) to form a total of

University of Delaware Department of Chemical and Biomolecular Engineering, Center for Neutron Science, 150 Academy St., Newark, DE, USA.
E-mail: srogers@udel.edu; Fax: +1 302-831-1048; Tel: +1 302-831-8079
† Present address: University of Illinois at Urbana-Champaign, Department of Chemical and Biomolecular Engineering, 600 S. Matthews Ave., Urbana, IL, USA. Tel: +1 217 333 0020; E-mail: sarogers@illinois.edu

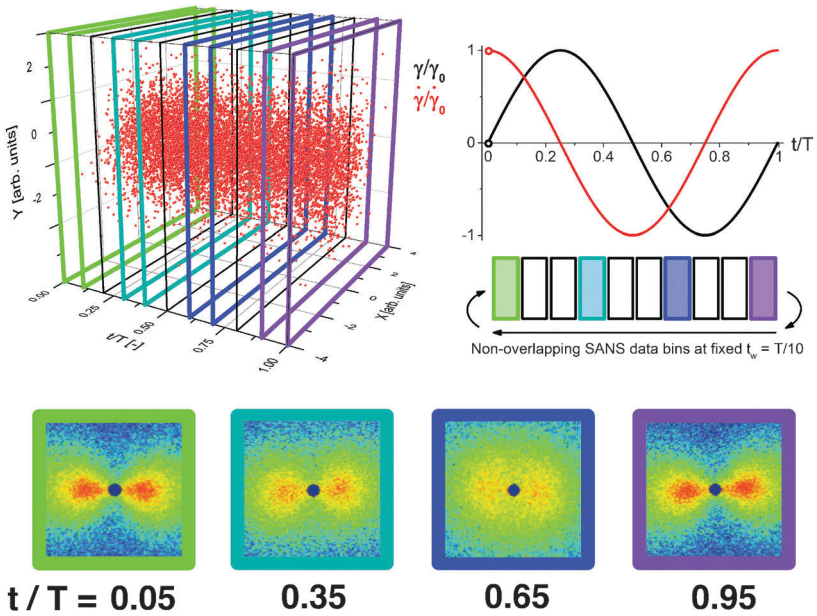

Fig. 1 Example time-resolved neutron scattering experiment of period T, where the detector records the spatial X and Y positions, and time of detection, for each scattered neutron. Each red dot represents an individual scattering event. The standard binning method for an oscillatory shear experiment groups neutrons registered within an interval of time, t_w, together (indicated by colored and black lines), forming a single scattering pattern with temporal resolution t_w. Here, $t_w = T/10$. Note the two temporal ends of the figure are joined, such that $t/T = 0 = 1$.

ten scattering patterns over the experiment period, T. By using the standard binning method, all derived material properties have an equal temporal resolution and precision of t_w. The temporal precision of the binned data is determined by the bin width, t_w, whereas the temporal resolution is determined by the time step between consecutive bins, which in the standard binning method is also t_w. Any properties that are changing on time scales faster than t_w cannot be detected. The scattering patterns shown result from the data binned between each set of colored lines and contain information about the material properties during that specific portion of the oscillation. In the previous example of a 30 minute scattering experiment with a bin width of one-minute, the standard binning method would result in 30 total bins each of duration one minute. Any structure changes occurring faster than one minute would not be detected using this method.

Processing time-dependent scattering

The data binning procedure is analogous to applying a moving average to a time series, as they both result in smoothed, time-averaged data. However, unlike in the moving average procedure, the data binning procedure is necessary to examine time-resolved data, as the material response cannot be elucidated without data processing. The goal of the time-resolved data analysis, therefore, is to resolve the underlying material response. In the context of time-resolved scattering experiments, the coarse-grained binning procedure is necessary to reduce the dimensionality of the data for analysis. In many cases, the binned data is referred to as being the 'true' material response, which is not accurate because the binned data depends on the choice of bin width. The true material response should be independent of the analysis method. By applying an ever-widening bin-width to the same experimental data, the finer features of the response will be 'averaged out' until eventually the bin is the same width as the period. Thus to determine the true material response, the method of analysis should account for, and remove, artifacts associated with the coarse graining procedure.

Convolution and deconvolution

Suppose that the underlying material response of interest, $m(t)$, is continuous and is represented by time-resolved elastic scattering data. The material response of interest could be the intensity or position of a particular peak, for example, or some integral function of the pattern such as an alignment factor or order parameter. These responses necessarily change as a function of real time throughout the experiment, and may be brought about from external forces such as shear or temperature change. This time-dependent response, $m(t)$, is not to be confused with the instrument resolution function or the material scattering function, which are defined in the inverse space domain. These functions are inherent to the instrument and the scattering data and are convolved in the inverse space domain, resulting in the instrument-smeared signal that is recorded during a scattering experiment. The function $m(t)$ therefore describes the time-dependent nature of the instrument-smeared signal; the following procedure does not attempt to alter or correct the signal based on instrument smearing. We also note that a finite wavelength distribution of neutrons in SANS experiments introduces time smearing of the response and this is not explicitly considered here, such that the method may require additional considerations for experiments performed with a broad distribution of incident

velocities, such as in a spallation neutron experiment. The scattering data is grouped into time bins, $b(t,t_w)$, of duration t_w, which is defined by the boxcar function at a time, t,

$$b(t, t_w) = \frac{1}{t_w}H\left(-t - \frac{t_w}{2}\right) - \frac{1}{t_w}H\left(-t + \frac{t_w}{2}\right) \quad (1)$$

where

$$H(t) = \int_{-\infty}^{t} \delta(s)\mathrm{d}s \quad (2)$$

is the Heaviside step function, and $\delta(s)$ is the Dirac delta function. The use of this bin function ensures that all neutrons inside the bin are counted with equal weighting, while those outside are ignored. The binned data, referred to as $c(t)$, is equivalent to the area overlap between the material response and the bin as a function of the amount that the bin is translated,

$$c(t) = \int m(t')b(t - t', t_w)\mathrm{d}t'. \quad (3)$$

Eqn (3) is more concisely written as

$$c(t) = m(t) \otimes b(t,t_w) \quad (4)$$

where $\otimes$ is the convolution operator. Eqn (4) therefore explicitly states that the binned data is the convolution of the material response and the bin. In order to obtain the material response $m(t)$, from the convolved data, $c(t)$, a deconvolution must be applied. According to the convolution theorem, the Fourier transform of a convolution is equal to the product of the Fourier transforms. Denoting the Fourier transform operator as $\mathscr{F}$, and the Fourier transform of a time domain function by a change of variable and capitalization, the theorem states that

$$\mathscr{F}\{c(t)\} = C(\omega) = \mathscr{F}\{m(t) \otimes b(t,t_w)\} = M(\omega)\cdot B(\omega,t_w). \quad (5)$$

In order to bin the data, a value of t_w in eqn (3) is chosen. Accordingly, $b(t,t_w)$ and $B(\omega,t_w)$ in eqn (4) and (5) are fully known. Given the form of the bin, as defined in eqn (1), the Fourier transform is the well-known sinc function,

$$\mathscr{F}\{b(t, t_w)\} = B(\omega, t_w) = \frac{2\sin\left(\frac{t_w\omega}{2}\right)}{t_w\omega}. \quad (6)$$

No assumptions, other than continuity in time, are made about the form of $m(t)$ or $M(\omega)$. To remove any artifacts associated with the binning procedure, the Fourier transform of the convolved (binned) data can be divided by the known Fourier transform of the bin,

$$M(\omega) = \frac{C(\omega)}{B(\omega, t_w)}. \quad (7)$$

The deconvolution, obtained by applying the inverse Fourier transform, results in replication of the material response unaffected, in principle, by any effects of the binning procedure,

$$\mathscr{F}^{-1}\{M(\omega)\} = \mathscr{F}^{-1}\left\{\frac{C(\omega)}{B(\omega, t_w)}\right\} = m(t). \quad (8)$$

The differences between the binning procedure and the full deconvolution process are illustrated for a time-periodic material response in Fig. 2(a) and (b), respectively, for bins of different sizes on a simulated data set. Only the first half of the period is shown in Fig. 2 for clarity. The simulated material response (black, Fig. 2(a) and (b)) is constructed of odd harmonics of equal magnitude up to and including the 29th harmonic. The simulated response was convolved with different time windows to obtain the results in Fig. 2(a); these results were then deconvolved by the same time window in Fig. 2(b).

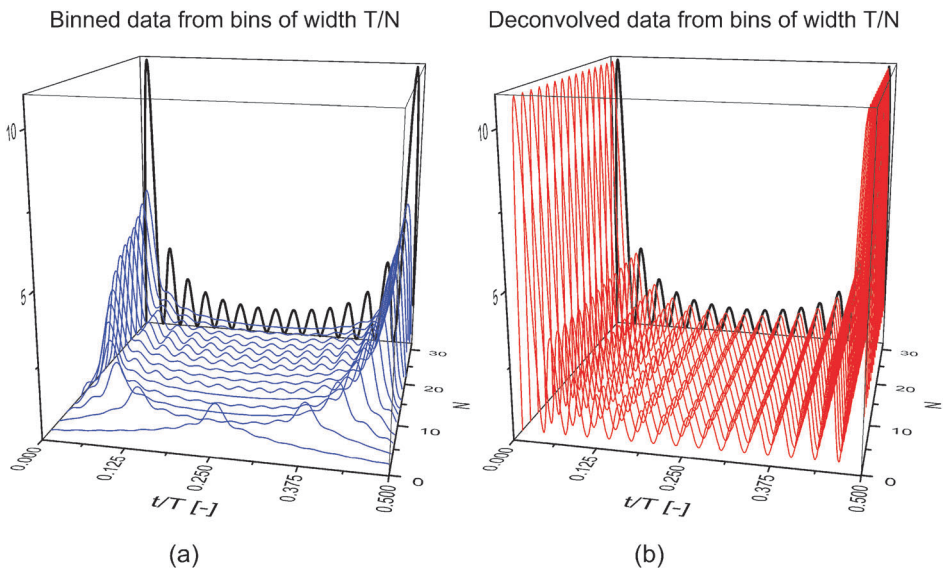

Fig. 2 The results of binning only (a) and binning and deconvolving (b) time-resolved sample data set from bins of width T/N, where T is the period of oscillation and N is an even integer. Only the first half of the oscillation is shown for clarity. The solid black line indicates the underlying material function, and the colored lines indicate the results of the two procedures. Only by deconvolution can the true material response be determined without artifacts from the analysis.

The results in Fig. 2(a) represent the material response that is obtained when different bin sizes are chosen to process the data. For convenience, the bin duration, t_w, is expressed as an even integer fraction of the period of oscillation, T, such that $t_w = T/N$. Here, the temporal resolution is approximately continuous through t/T, whereas the temporal precision is determined by the bin width, T/N. Larger integers thus correspond to shorter bins, better approximating the underlying material response. Clearly, the results of binning alone are dependent on the bin size, as significantly different responses are seen with changing N. In Fig. 2(b), the data from Fig. 2(a) is deconvolved to obtain the true material response. The result of the deconvolution is completely independent of the bin size, a property required of the material response.

On the basis of the data displayed in Fig. 2, a bin as wide as half of the period, $T/2$, can be used, in theory, to accurately determine the material response *via* deconvolution. Such analysis has clear implications in the length of time required to carry out a time-resolved scattering experiment. In many studies where binning is used, bin widths on the order of $T/30$ are employed to provide a reasonable balance between temporal resolution and experiment duration.[5,14] If a constant number of scattering events per bin is desired (normally around 100 000 –250 000 or greater, depending on the information sought by the researcher), then scattering events sufficient to fill bins of width $T/2$ can be collected 15 times faster than the number of scattering events required to fill bins of width $T/30$. However, experimental limitations and noise in the data limit the practical bin size that can be applied to reduce scattering time, which will be discussed in the next section.

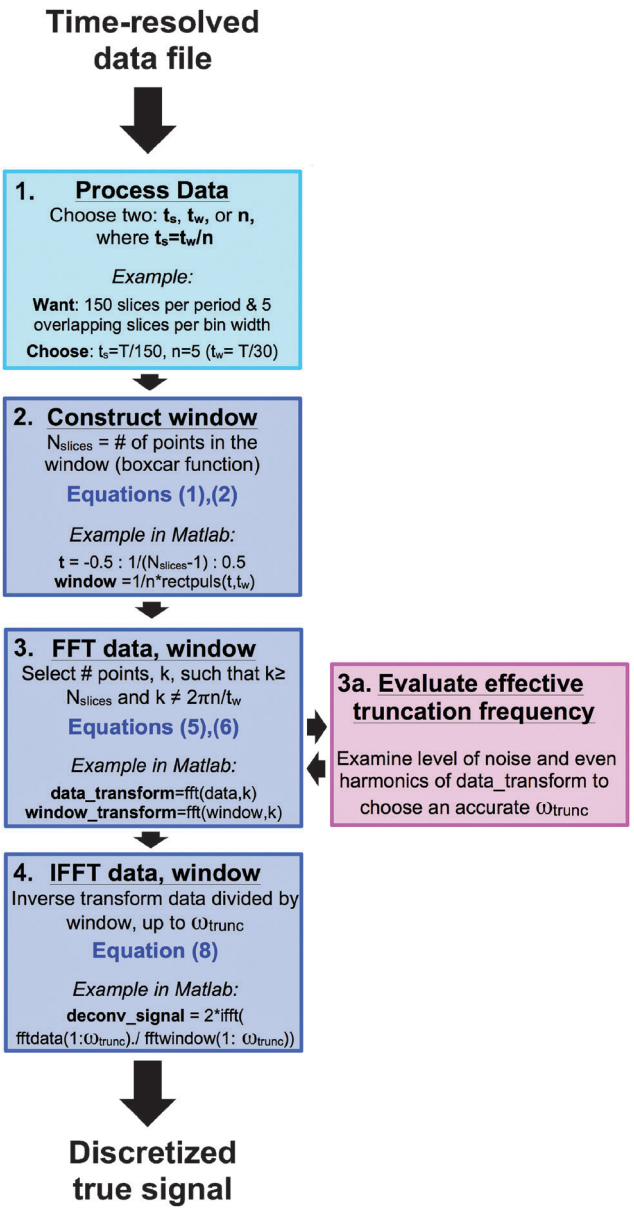

Fig. 3 Flow chart illustrating the data processing and deconvolution procedure, with a Matlab example for reference. Steps 2 to 4. Correspond to equations discussed in the text, whereas step 1. Is performed in the scattering reduction software. Step 3a allows the user to determine the optimal truncation frequency for the inverse transform.

Discretization

The formalism above in support of deconvolution assumes continuous functions and transforms. Practically, the underlying continuous material response can only be measured discretely, and therefore, the 'true' deconvolved signal must also be discrete. The integrals in eqn (3) and those involved in the transforms in eqn (5) and (8) are therefore replaced by sums. While the arguments remain the same, the application of the ideas requires refinement when dealing with discretely-measured data. The primary concerns when deconvolving discrete data are associated with Fourier transformation and inverse Fourier transformation, which can be affected by noise, time-step size, and bin-width. Additionally, the binned data must be processed in a specific manner to implement the deconvolution procedure. In the standard binning method, the temporal precision and temporal resolution are the same because the bins are non-overlapping in time. Accordingly, the binned material response cannot be deconvolved because there exists only one data point per bin width. The binning procedure can be modified to allow the bins to 'slide' at a certain time step, t_s, where $t_s \ll t_w$. In this method, referred to as the sliding binning method, the bins overlap in time so that neutrons are counted multiple times, but only once per bin. Implementing the sliding binning method greatly increases the temporal resolution of the binned signal (by a factor of $n = t_w/t_s$), thus enabling better deconvolution. In the previous example of a 30 minute scattering experiment with a bin width of one-minute, the sliding binning method increases the total bin number by $30n$. A chosen value of $n = 5$ would result in 150 total bins, each of duration one minute (illustrated in Fig. 3). Note that the appropriate choice of n is dependent on the data set, and larger n-values are often required for wider bin widths. This numerical example, given in step 1. of Fig. 3, uses the sliding binning method to achieve five-fold improved temporal resolution over the standard binning method. Fig. 3 also helps to visualize the full procedure, from the data processing to the final

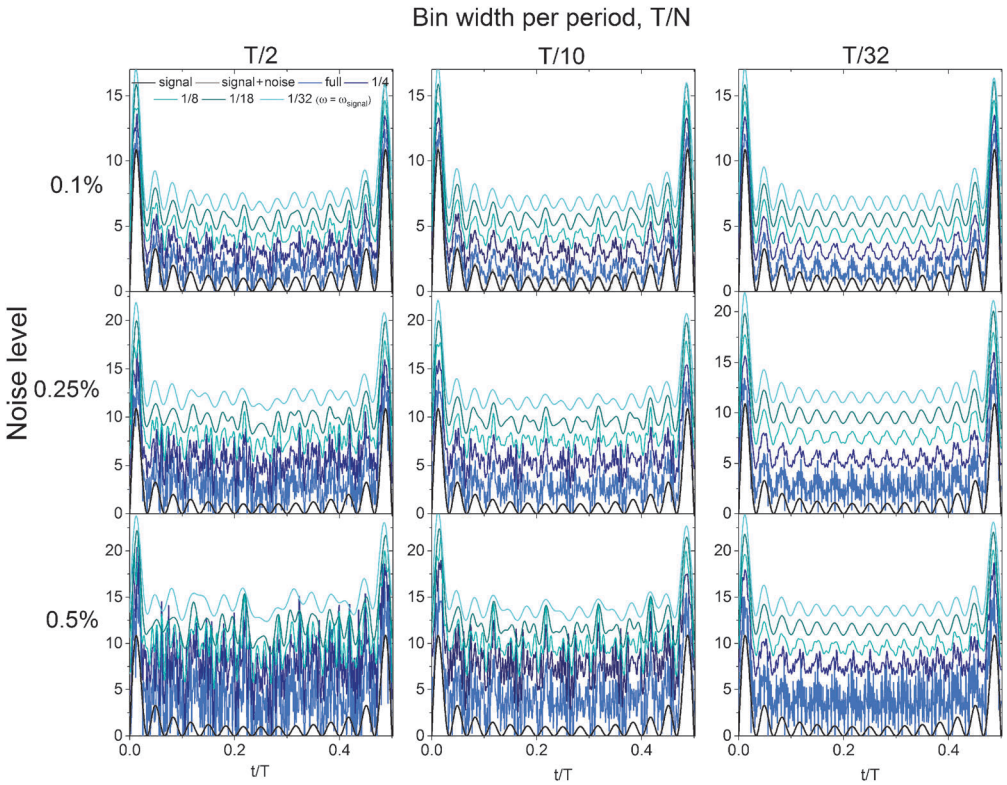

Fig. 4 Binning and deconvolution of noisy data at different bin (time) widths. Noise levels of 0.1, 0.25 and 0.5% were added to the time-average of the original signal from bin widths of $T/2$, $T/10$ and $T/32$. The full frequency spectrum transform always returns noisy data. However, truncating the Fourier transforms (denoted as a fraction of the full spectrum) removes noise from the signal so that the true signal is more closely approximated. The original signal (black) has frequencies corresponding to 1/32 of the full Fourier transform. The true signal at 1/32 of the full transform is best approximated using bins of $T/32$, and deviates significantly with increasing bin size. Data is shifted vertically for visual aid.

deconvolution step. A sample procedure and Matlab commands are provided as a practical example, which addresses issues such as noise and bin width effects (which will be discussed below).

Noise effects

The deconvolution process provides a pathway for dramatically reducing the acquisition time for a time-resolved scattering experiment by using larger bin sizes. However, noise effects limit the practical bin width that can be applied to a data set to obtain an accurate deconvolved signal. Fourier transforming discrete data requires division by the number of points in the time domain signal, and inverse Fourier transformation requires multiplication by the number of points in the frequency domain signal. The signal-to-noise ratio (SNR) of an experimentally-measured signal can be increased by truncating the spectrum in the frequency domain. Truncating the frequency spectrum is almost always necessary based on the noise level and the error associated with experimental data (step 3a, Fig. 3). In time periodic experiments, the truncation frequency can be estimated by examining the magnitude of the noise in the Fourier transform of the time-averaged data, which is most apparent at high frequencies. Truncating the full spectrum thereby removes a significant amount of noise from the signal. The inverse Fourier transform then only uses the frequencies that are above the level of the noise to reconstruct the discrete true signal. In data sets where the noise amplitude is higher than that of a frequency that contributes to the signal, the feature resulting from that frequency cannot be resolved in the true signal. Fig. 4 examines the effect of noise on the deconvolution procedure for different bin widths and different truncation frequencies.

The signals in Fig. 4 are calculated by deconvolving the time-average of the original signal featured in Fig. 2 with different levels of added noise. These calculations are the same as those performed in Fig. 2; however noise was added to the time-averaged signal before performing the deconvolution, such that the results are no longer analytically defined. Gaussian-distributed zero-mean white noise was generated in Matlab, where one standard deviation of the noise amplitude was equal to 0.1%, 0.25% or 0.5% of the mean amplitude of the time-averaged signal. Fig. 4 clearly shows the effect of noise on the deconvolved signal at different bin widths ($T/2$, $T/10$, $T/32$), and of truncating the full Fourier spectrum at different frequencies, ranging from the full frequency spectrum (no truncation) to 1/32 of the full spectrum (number of frequencies used to construct the original signal). As seen in Fig. 4, the closer the truncation frequency is to the number of frequencies used to generate the signal, the more noise is filtered, leading to a smoother signal. However, the end of the Convolution and deconvolution section illustrated a case where a bin width of $T/2$ can reduce the time that would currently

be taken to acquire data sufficient for bins of width $T/30$ by a factor of 15. However, as Fig. 4 shows, there are limitations in the bin width that should be chosen when performing an experiment. Bins of width $T/32$ handle the noise the best, as the smaller bin width leads to sharper features in the time-averaged signal, which results in a high signal-to-noise ratio. Using bins of $T/32$, the deconvolution result after truncation is nearly unaffected by the increasing noise level within the range examined. However, the effect of the added noise is pronounced at bins of $T/2$, where even the truncated deconvolution results greatly differ from the expected original signal. Smaller bin widths are optimal in the deconvolution procedure for several reasons. The width of the sinc function in frequency space is inversely proportional to the bin width in real time, meaning that smaller bin widths cover a wider frequency range. The number of roots in the sinc function also increases with wider bin sizes in the same frequency range, leading to more information loss with wider bins. Lastly, the amplitude of the sinc function at high frequencies is larger when the bin size is smaller, leading to a the higher signal-to-noise ratio when the deconvolution is performed. However, by truncating the spectrum at all bin widths, the deconvolution result becomes closer to that of the original signal. The truncation of the frequency spectrum is important to perform during this procedure (Fig. 3 and 4) such that only the frequencies with amplitudes significantly above the level of the noise are used to reconstruct the discrete true signal.

Time-step size effects

A fundamental result in the field of information theory, often referred to as the Nyquist–Shannon sampling theory states that

If a function $x(t)$ contains no frequencies higher than B Hz, it is completely determined by giving its ordinates at a series of points spaced $1/(2B)$ s apart.

The sampling theorem sets the upper limit on the angular frequencies that can be determined by the Fourier transformation of discretely-measured data. The upper frequency limit of the band, denoted by B, and the size of the time step, t_s, are therefore related by:

$$B = \frac{\pi}{t_s}. \tag{9}$$

The frequency response of the bin function defined in eqn (1) decays with angular frequency as $\frac{2}{t_w\omega}$ as shown in eqn (6). In the deconvolution, the Fourier transform of the convolved data is therefore divided by a number less than or equal to one. It is possible to set a value on how much the frequency response has decayed by truncating the response at a particular frequency. If we refer to the amplitude of the sinc function as L:

$$L = \frac{2}{t_w\omega} \tag{10}$$

The frequency that solves eqn (10) can be readily equated with the upper frequency of the band from eqn (9) to give a relation between the step size, the bin width, and the desired amplitude of the sinc function,

$$\frac{2}{Lt_w} = \frac{\pi}{t_s} \Rightarrow \frac{t_w}{t_s} = \frac{2}{\pi L}. \tag{11}$$

This result states that if one wishes to probe frequencies as high those required to decay the sinc function to 5% of the zero-frequency value, such that $L = 0.05$, then $\frac{t_w}{t_s} = \frac{40}{\pi} \approx 12.73$. This requires the step size to be thirteen times smaller than the bin width. However, often times the experimental scattering signal decays much faster than that of the sinc function. In oscillatory shear experiments, for example, the stress response is highly indicative of the scattering signal. The higher order harmonics present in the Fourier transform of the stress response are a good estimate of the higher order harmonics present in the structural response. In many of these experiments, it is more realistic to decay the sinc function to 15–20% of the zero-frequency value, where the frequency of the sinc function is near that of the data truncation frequency (determined using step 3a in Fig. 3). At 15–20% of the zero-frequency value, a step size of $t_s = t_w/3$ or $t_w/5$ is often sufficient; however, the optimal step size is dependent on the data set and bins of large t_w may require finer step sizes.

Bin-width effects

In addition to the amplitude, the phase of the sinc must also be considered to determine which frequencies will be irretrievably lost during the deconvolution. As $\sin(\omega) = 0$ when $\omega = n\pi \; \forall \; n \in \mathbb{Z}$, frequencies equal to $\frac{n2\pi}{t_w}$ will be eliminated from the deconvolved function. Practically speaking, the deconvolution will be undefined when the discrete Fourier transform (DFT) of the time window contains zeros, as the DFT of the time-averaged data is divided by that of the window function. As mentioned in Fig. 3, the number of points for the transform can be carefully chosen to avoid such complications. Note that the chosen number of points for the transform, k, should be greater than or equal to the number of slices. By doing so, the transform will be padded with zeros (Matlab), as opposed to prematurely truncating the spectrum.

Experimental results and accessibility

The standard and proposed analysis techniques are compared using a time-resolved large amplitude oscillatory shear (LAOS) rheo-SANS experiment taken at the National Institute of Standards and Technology Center for Neutron Research (NCNR). The experiment was performed on a previously characterized[15,16] mildly branched wormlike micellar solution with an applied strain amplitude $\gamma_0 = 225$ and angular frequency $\omega = 0.2$ rad s^{-1}. Scattering was measured in the 1,3 flow-vorticity plane of shear. One material property that is directly calculated from binned neutron data, which therefore may represent $c(t)$, is the alignment factor. The scalar alignment factor is a measure of shear-induced

segmental alignment (anisotropy) and is defined by the spatial average on the detector, given by,

$$A_f = \frac{\int_0^{2\pi} I(q,\phi)\cos(2(\phi-\phi_0))d\phi}{\int_0^{2\pi} I(q,\phi)d\phi} \quad (12)$$

where $I(q)$ is the intensity over a small fixed q-range, ϕ is the azimuthal angle, and ϕ_0 is the azimuthal angle of maximum intensity. This average is calculated over a finite range of scattering vectors based on a specific physical feature of interest.

Fig. 5 shows the results for the standard binning method, the sliding binning method, and the full deconvolution (translated for visual aid). First, the alignment factor was calculated for each of the thirty, non-overlapping bins (red) using the standard binning method ($t_w = t_s = T/30$). The sliding binning method (gray) was performed on the same data set using overlapping bins with a step size five-fold smaller than the bin width ($t_w = T/30$, $t_s = T/150 = t_w/5$), yielding a five-fold improvement in the temporal resolution and 150 total bins. While a value of $n = 5$ (as seen in Fig. 3) provides sufficient temporal resolution to perform the deconvolution for bins of width $T/30$ in this experiment, larger values of n may be required when the chosen bin size is larger than $T/30$. The experimental data processed using the sliding bin method (gray) was then deconvolved to elicit the true (discretized) material response (black). The discrete nature of the standard binning method, which leads to poor temporal resolution, is apparent in Fig. 5, whereas the sliding binning method presents improved temporal resolution. The sliding bin curve (gray) exhibits small oscillations in the alignment factor signal, suggestive of a higher frequency material response, that are not seen with the standard binning method. While portions of the sliding bin curve could be interpolated from the standard bin points, the existence of the higher frequency oscillations in the material structure and the position and value of the maximum alignment would not be resolvable *via* interpolation. The deconvolved signal (black) displays sharper oscillations in A_f that reflect the true material alignment. The residuals in Fig. 5 highlight the improvements to feature sharpness and quality obtained by the deconvolution procedure.

In Fig. 6, we examine the higher frequency oscillations in the alignment factor and compare the deconvolved, true alignment (black) to the measured shear stress (blue). The alignment factor oscillations clearly correspond to similar oscillations in the measured shear stress. These features cannot be resolved using the standard binning method due to poor temporal resolution and limited number of points, making it more difficult to derive information from the stress-SANS law,[17] or other empirical relationships. Simply reducing the bin size will not improve the situation, as the statistical accuracy of the data decreases correspondingly. The improved temporal resolution and feature clarity gained from the deconvolution provide a

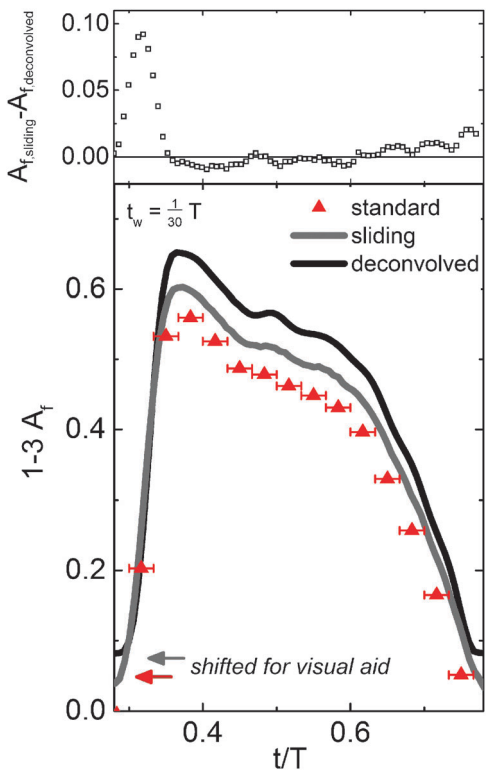

Fig. 5 Experimental results from a mildly branched wormlike micellar solution under LAOS at $\omega = 0.2$ rad s^{-1} and $\gamma_0 = 225$ ($\dot{\gamma}_0 = 45$ s^{-1}). The time periodic 1–3 plane alignment factor, $c(t)$, is binned into 150 bins of width $t_w = T/30$ ($t_s = t_w/5$). The standard binning method (red) is compared to the sliding binning method (gray) and the full deconvolution (black). Small oscillations in the alignment factor signal from $0.45 < t/T < 0.65$ are not resolved using the standard binning method. The residuals between the methods show the impact of the deconvolution procedure, where the deconvolved signal exhibits sharper, more pronounced oscillations that represent the true material alignment. Error bars span the bin time width.

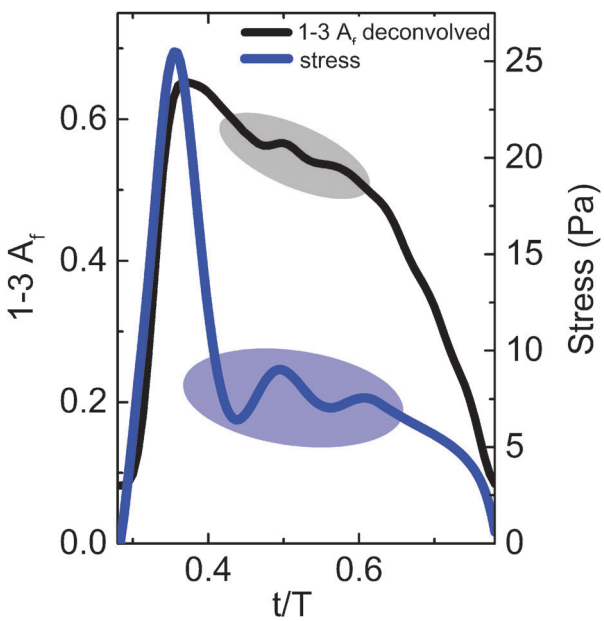

Fig. 6 Comparison of the deconvolved signal (black) and the material shear stress response (blue). The oscillations detected in the deconvolved signal directly reflect the features in the stress response. The enhanced temporal resolution and sharpness of the features gained by deconvolution enables quantitative relationships to be developed between the alignment and stress.

more direct and accurate pathway to quantitatively link the structural alignment to the measured bulk rheological properties. The deconvolution process also provides a method for reducing total experiment time required to achieve a given accuracy in scattering experiments. However, the noise level ultimately limits the resolution that can be obtained. Similar to the results shown in Fig. 4, the experimental deconvolution results for this data set are insensitive to bins of width $T/20$ compared with $T/30$ (data not shown), leading to a reduction in scattering (data acquisition) time of one-third.

In additional oscillatory shear conditions, we found that the deconvolution results were also unaffected by the reduction in bin width from $T/30$ to $T/20$ (data not shown). Depending on the features present in the signal, further time reduction can be obtained by implementing larger bin sizes. The time-averaged signal in Fig. 6 has two small oscillations on the order of $T/10$ in the alignment factor and stress signal: one from $0.45 < t/T < 0.55$ and the other from $0.55 < t/T < 0.65$. Therefore, when a bin size on the order of $T/10$ is used, the magnitude of the Fourier transform at these frequencies is roughly equivalent to the noise, making an accurate deconvolution difficult to perform. As the material stress response contains complementary features to the alignment factor response, the appropriate bin width can be estimated by examining the width of the stress response features and then choosing a smaller bin size. By decreasing the bin size from $T/10$ to $T/20$, the deconvolution was successfully performed for this data set.

In summary, we have shown a procedure to determine the true, underlying material response from a time-periodic signal given discrete data points, such as the alignment factor calculated from neutron events. This is accomplished by rigorously deconvoluting the scattering data, which is unavoidably operated on by a sliding boxcar function in time during data processing. When applied to a particular time-resolved data set, the proposed sliding bin method gives the same temporal precision as the standard bin method, while greatly improving the temporal resolution. The full deconvolution procedure yields the true material response, which is unobtainable using binning alone. This procedure is general and can be applied to many forms of time-periodic scattering data.

Conclusions

An improved method of analyzing time-resolved elastic scattering data is shown to increase the precision of the functions derived from scattering information, while significantly decreasing the data acquisition time. The developed deconvolution procedure greatly improves the temporal resolution and the resulting accuracy of the calculated material response to an external excitation. Sample data sets with and without noise and SANS measurements taken during large amplitude oscillatory shear show that the experiment time can be reduced by one-third or more, depending on the time scale of the features. The improved accuracy and precision of the deconvolved signal features enable the scattering signal to be quantitatively linked to the measured rheology for the development of structure–property relationships.

Acknowledgements

We acknowledge the support of the National Institute of Standards and Technology, U.S. Department of Commerce, in providing the neutron research facilities used in this work. This manuscript was prepared under cooperative agreement 70NANB12H239 from NIST, U.S. Department of Commerce. The statements, findings, conclusions and recommendations are those of the author(s) and do not necessarily reflect the view of NIST or the U.S. Department of Commerce.

References

1 D. I. Svergun, M. H. Koch, P. A. Timmins and R. P. May, *Small angle X-ray and neutron scattering from solutions of biological macromolecules*, Oxford University Press, 2013, vol. 19.
2 S. M. Perera, U. Shrestha, U. Chawla, A. V. Struts, S. Qian, M. F. Brown and X.-Q. Chu, *Biophys. J.*, 2014, **106**, 634a.
3 T. Nishida, A. Obayashi, K. Haraguchi and M. Shibayama, *Polymer*, 2012, **53**, 4533–4538.
4 M. E. Helgeson, S. E. Moran, H. Z. An and P. S. Doyle, *Nat. Mater.*, 2012, **11**, 344–352.
5 J. M. Kim, A. P. Eberle, A. K. Gurnon, L. Porcar and N. J. Wagner, *J. Rheol.*, 2014, **58**, 1301–1328.
6 G. Nagy, L. Kovács, R. Ünnep, O. Zsiros, L. Almásy, L. Rosta, P. Timmins, J. Peters, D. Posselt and G. Garab, *Eur. Phys. J. E: Soft Matter Biol. Phys.*, 2013, **36**, 1–12.
7 S. Mahabir, D. Small, M. Li, W. Wan, N. Kučerka, K. Littrell, J. Katsaras and M.-P. Nieh, *Biochim. Biophys. Acta, Biomembr.*, 2013, **1828**, 1025–1035.
8 M. Fumagalli, S. Lyonnard, G. Prajapati, Q. Berrod, L. Porcar, A. Guillermo and G. Gebel, *J. Phys. Chem. B*, 2015, **119**, 7068–7076, DOI: 10.1021/acs.jpcb.5b01220.
9 S. Jaksch, A. Schulz, K. Kyriakos, J. Zhang, I. Grillo, V. Pipich, R. Jordan and C. M. Papadakis, *Colloid Polym. Sci.*, 2014, **292**, 2413–2425.
10 F. Kaneko, A. Radulescu and K. Ute, *Polymer*, 2013, **54**, 3145–3149.
11 D. Q. Ly, T. Honda, T. Kawakatsu and A. V. Zvelindovsky, *Macromolecules*, 2007, **40**, 2928–2935.
12 F. Michaux, N. Baccile, M. Impéror-Clerc, L. Malfatti, N. Folliet, C. Gervais, S. Manet, F. Meneau, J. S. Pedersen and F. Babonneau, *Langmuir*, 2012, **28**, 17477–17493.
13 S. Rogers, J. Kohlbrecher and M. Lettinga, *Soft Matter*, 2012, **8**, 7831–7839.
14 A. K. Gurnon, C. R. Lopez-Barron, A. P. Eberle, L. Porcar and N. J. Wagner, *Soft Matter*, 2014, **10**, 2889–2898.
15 B. A. Schubert, E. W. Kaler and N. J. Wagner, *Langmuir*, 2003, **19**, 4079–4089.
16 M. A. Calabrese, S. A. Rogers, R. P. Murphy and N. J. Wagner, *J. Rheol.*, 2015, **59**, 1299–1328.
17 M. E. Helgeson, P. A. Vasquez, E. W. Kaler and N. J. Wagner, *J. Rheol.*, 2009, **53**, 727–756.

